Indian Journal of Chemistry
Vol. 56A, October 2017, pp. 1028-1033

# Structure and photocatalytic activity of bismuth tungstate nanoparticles synthesized by one-step solvothermal method

Xiang-Hui Zhang

Henan Key Laboratory of Electromagnetic Transformation and Detection, College of Physics and Electronic Information, Luoyang Normal University, Luoyang, 471934, PR China

Email: zxhlynu@163.com

*Received 14 August 2017, revised and accepted 27 September 2017*

$Bi_2WO_6$ has been synthesized by water, methanol or ethylene glycol assisted solvothermal method. The physical and photophysical properties of the as-prepared samples are characterized by XRD, UV-vis, SEM and BET surface area measurements. XRD results show orthorhombic $Bi_2WO_6$ with the average crystallite size of about 9.2 nm, obtained using ethylene glycol as the reaction solvent. By substituting ethylene glycol for deionized water or methanol as solvent, the size of $Bi_2WO_6$ increases. BET results indicate that the $Bi_2WO_6$ sample prepared in ethylene glycol has the largest surface area (56.5 $m^2$ $g^{-1}$). The photocatalytic activities of as-prepared samples have been evaluated by the degradation of methylene blue in an aqueous solution under visible light irradiation. The degradation ratio of MB over $Bi_2WO_6$ synthesized in ethylene glycol (97.1%) is much higher than that over $Bi_2WO_6$ synthesized in deionized water (82.8%) and methanol (50.0%) within 120 min. This may be attributed to its appropriate energy band structure, small crystallite size, and high surface area.

**Keywords:** Bismuth tungstate, Ethylene glycol, Methylene blue, Dye degradation, Solvothermal method

Environmental pollution has become one of the most critical problems for human beings, and therefore a variety of technologies have been developed to solve the environmental problems. Among these technologies, photocatalytic technology has the advantages of high stability, corrosion resistance, non-toxicity and no secondary pollution. Therefore, this technology is efficient and energy-saving and also has extensively applied prospects in pollutant control.[1-3] The efficient utilization of energy and degradation of target contaminants are the important link to solve the pollution problem. The key to realize this is to develop high efficiency and stable photocatalysts.

$TiO_2$ is the most studied and efficient photocatalyst presently known. However, it can only respond to ultraviolet light due to its wide band gap, resulting in a very low efficiency of utilization of sunlight.[4] In order to use sunlight more efficiently, developing photocatalysts capable of responding to visible light has become the urgent need in the field of photocatalysis. Many types of visible light-responding photocatalytic materials have been developed by various methods, such as doped $TiO_2$,[5] $Cd_xZn_{1-x}S$,[6,7] $ZnIn_2S_4$,[8] $WO_3$,[9] $Ag_3PO_4$,[10] $Bi_2WO_6$,[11-13] etc. Among these photocatalysts, $Bi_2WO_6$ has attracted more and more attention in recent years due to its good photocatalytic performance in water splitting and decomposition of organic pollutant under visible light irradiation. $Bi_2WO_6$ is one of the simplest members of the Aurivillius family. It is composed of alternating $(Bi_2O_2)^{2+}$ layers and $(WO_4)^{2-}$ octahedral layers.[14] This unique layered structure leads to carriers migrating to the surface quickly, and thus improving the transfer efficiency of photogenerated carriers. Therefore, the photocatalytic activity is promoted. Moreover, the Bi 6*s* and O 2*p* hybrid orbitals form the valence band and W 5*d* orbital forms the conduction band of $Bi_2WO_6$.[15] Due to hybridization between Bi 6*s* and O 2*p* orbital, the valence band potential of $Bi_2WO_6$ rises, and the forbidden band decreases. Thus $Bi_2WO_6$ displays excellent photocatalytic activity under visible light irradiation.

Since the photocatalytic activity of $Bi_2WO_6$ is closely related to factors such as phase structure, synthetic method, grain size and particle morphology, the controlled synthesis of $Bi_2WO_6$ with regular morphology and high visible light photocatalytic activity has been the focus in recent years. Liquid phase chemical synthesis techniques, especially

hydrothermal and solvothermal techniques have become one of the most promising methods due to the simple operation, mild reaction, high efficiency and low cost. It has been widely used successfully in the synthesis of inorganic nanomaterials. Zhang *et al.*[16] have prepared lamellar $Bi_2WO_6$ via cetyltrimethylammonium bromide (CTAB) assisted hydrothermal synthesis. Zhao *et al.*[17] have successfully synthesized the flower-like $Bi_2WO_6$ by the hydrothermal method using CTAB. Liu *et al.*[18] have synthesized one-dimensional hierarchical $Bi_2WO_6$ hollow tubes with porous walls by the solvothermal method using diluted acetic acid as solvent. Wang *et al.*[19] have successfully synthesized $Bi_2WO_6$ hollow microspheres by the solvothermal process using ethylene glycol and absolute ethanol as solvent. All these samples have shown good photodegradation performance for simulated studies.

From the above studies, it can be seen that the solvent influences the morphology and photocatalytic performance of $Bi_2WO_6$. By adjusting the control parameters the preparation of nanomaterials with a particular morphology can be achieved. However, there is little research on the effect of solvents on the crystal structure and photocatalytic activity of $Bi_2WO_6$. Using deionized water (DIW), ethylene glycol (EG) and methanol (MT) as solvent in this study, $Bi_2WO_6$ photocatalysts have been prepared by a one-step solvothermal method. The influence of solvents on the physical properties and photocatalytic efficiency of the photocatalyst are studied. Among these samples, $Bi_2WO_6$ prepared in EG showed higher methylene blue (MB) photodegradation activity than the samples prepared in DIW or MT. Finally, the reasons of the photocatalytic activity increased were systematically analyzed.

## Materials and Methods

### Preparation and characterization of photocatalysts

All chemicals are analytical grade and used as received ones. The $Bi_2WO_6$ photocatalysts were prepared by a one-step solvothermal method in the absence of surfactants. Bismuth nitrate pentahydrate (2.91 g) and sodium tungstate dehydrate (0.99 g) were dissolved in 50 mL of deionized water, ethylene glycol or methanol, and transferred to a 100 mL Teflon-lined stainless autoclave. The autoclave was sealed and maintained at 433 K for 20 h, and then cooled to room temperature naturally. The obtained precipitate was filtered and washed with absolute ethanol and deionized water several times. After dying at 353 K in air, $Bi_2WO_6$ samples were obtained, and labeled as BWO-DIW, BWO-EG, and BWO-MT, respectively.

X-ray diffraction (XRD) patterns of the photocatalysts were recorded in a wide angle range ($2\theta = 20 - 70°$) on a Bruker D8 Advance X-ray diffractometer using Cu Kα irradiation ($\lambda = 1.5406$ Å). An accelerating voltage of 40 kV and emission current of 40 mA conditions were adopted for the measurements. The Brunauer-Emmett-Teller (BET) surface area was measured using a Micromeritics ASAP 2020 apparatus at liquid nitrogen temperature (77 K). The morphology of the photocatalysts was observed by Phenom Pro scanning electron microscope (SEM). UV-vis absorption spectra (UV-vis) were recorded on a Shimadzu UV-3600 plus UV-vis-near-IR spectrophotometer. The spectra were collected in the 240 – 800 nm range at room temperature using $BaSO_4$ as a reference.

### Photocatalytic reaction

The photocatalytic activity of $Bi_2WO_6$ samples was evaluated by the degradation of MB as a well-established standard dye in aqueous solution under visible light irradiation. A 300 W Xe lamp with a cut-off filter ($\lambda > 420$ nm) was used as the light source. The reaction was thermostated at 303 K with a water cooling jacket. In each experiment, 0.1 g of the photocatalyst was added to 200 mL of MB solution ($10^{-5}$ mol $L^{-1}$). Prior to irradiation, the suspensions were magnetically stirred in the dark for 30 min to ensure the establishment of an adsorption-desorption equilibrium between the photocatalyst and MB. Then the solution was exposed to irradiation under magnetic stirring. At every 30 min, 4 mL of the suspension was sampled and centrifuged to remove the photocatalyst particles. The degraded solutions of MB were analyzed by a Shimadzu UV-3600 plus UV-vis-near-IR spectrophotometer, and the absorption peaks at 664 nm for MB were monitored. The percentage of degradation is reported as $C/C_0$, where $C$ is the absorption of MB at each irradiated time interval of the maximum peak of the absorption spectrum at wavelength 664 nm, and $C_0$ is the absorption of the starting concentration when adsorption/desorption equilibrium was achieved.

## Results and discussion

### Crystal structure

Figure 1 shows the XRD patterns of $Bi_2WO_6$ samples prepared in different solvents. When DIW and EG were used as solvent, the diffraction peaks for

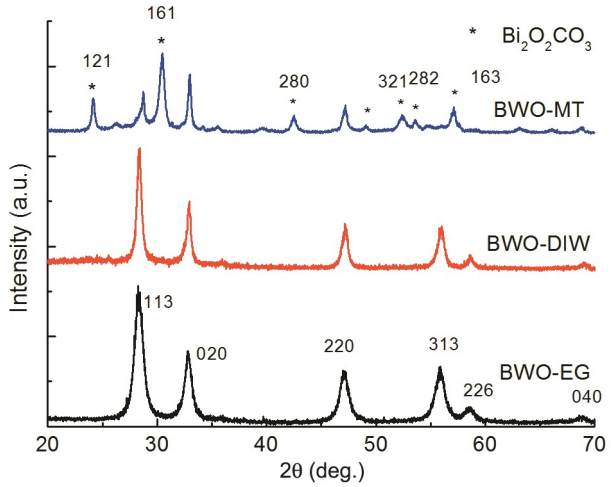


Fig. 1 — X-ray diffraction patterns of $Bi_2WO_6$ samples.

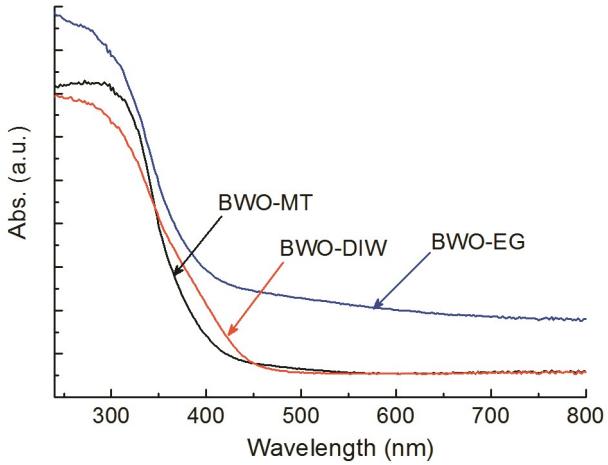


Fig. 2 — UV-vis spectra of $Bi_2WO_6$ samples.

both samples can be assigned to the orthorhombic phase of $Bi_2WO_6$ (JCPDS No. 73-1126, $a$ = 5.457 Å, $b$ = 5.436 Å, $c$ = 16.427 Å).[18] The diffraction peaks at $2\theta$ of 28.31°, 32.93°, 47.16°, 55.83°, 58.56° and 69.06° correspond to (113), (020), (220), (313), (226), and (040) planes of orthorhombic $Bi_2WO_6$. No other impurities such as $WO_3$, $Bi_2O_3$ or organic compounds related to the reactants were detected, indicating the high phase purity of synthesized $Bi_2WO_6$. However, the BWO-DIW sample exhibits narrower diffraction peaks than the BWO-EG sample because of the increase of crystallite size. Using the full width at half-maximum of XRD peaks at 28.31°, 32.93°, 47.16° and 55.83° with Scherrer equation, the average size is calculated to be 9.2 nm and 14.5 nm for BWO-EG and BWO-DIW, respectively. When MT was used as solvent, the product contained not only orthorhombic $Bi_2WO_6$ phase but also tetragonal $Bi_2O_2CO_3$ phase (JCPDS No. 41-1488).[20] The average crystallite size for the BWO-MT sample is calculated to be 26.5 nm by Scherrer equation. The reason of $Bi_2O_2CO_3$ formation may be as follows: $Bi(NO_3)_3 \cdot 5H_2O$ was heated and decomposed into $BiONO_3$ and $HNO_3$, and then $HNO_3$ oxidized $CH_3OH$ to generate $CO_2$, $H_2O$, etc. Finally, $BiONO_3$ reacted with $CO_2$ and $H_2O$ to form $Bi_2O_2CO_3$.

**UV-vis absorption spectra**

As is well-known, the optical properties of a semiconductor are related to its energy band structure, which plays a key role in determining the photocatalytic activity. The UV-vis absorption spectra of $Bi_2WO_6$ samples are shown in Fig. 2. As can be seen in the figure, the BWO-MT sample presents the photo-absorption property in ultraviolet light region. It may be attributed to the formation of $Bi_2O_2CO_3$, which has been demonstrated by XRD technique. However, the BWO-DIW and BWO-EG samples have intense absorption bands with steep edges from ultraviolet light region to visible light region. The steep absorbance bands of the spectra indicate that the visible light absorption is due to a band gap transition, not due to the transition from impurity energies to the conduction band.[21] Moreover, there is an enhanced light absorbance in the entire spectra in the visible light region for the BWO-EG sample, indicating the possibility of high photocatalytic activity. The band gap energy of the prepared samples was calculated from the onsets of absorption edges, and found to be 2.75 eV, 3.10 eV and 2.87 eV for BWO-DIW, BWO-MT and BWO-EG, respectively.

**Morphology**

Figure 3 shows the SEM images of the $Bi_2WO_6$ samples. From the SEM images, it can be seen that the as-prepared $Bi_2WO_6$ samples comprise aggregated clusters consisting of many nanoparticles about 10 – 40 nm. This result matches well with the average crystallite size derived from the XRD patterns described above.

**Surface area**

The BET surface area of the $Bi_2WO_6$ samples was also estimated by $N_2$ adsorption data, and found to be 24.8 $m^2\ g^{-1}$, 14.1 $m^2\ g^{-1}$ and 56.5 $m^2\ g^{-1}$ for BWO-DIW, BWO-MT and BWO-EG samples, respectively. The BET surface area of BWO-EG is much larger than that of BWO-DIW, while the BET surface area of BWO-MT is smaller than that of BWO-DIW. It is noteworthy that the photocatalytic performance of a photocatalyst is closely related to its

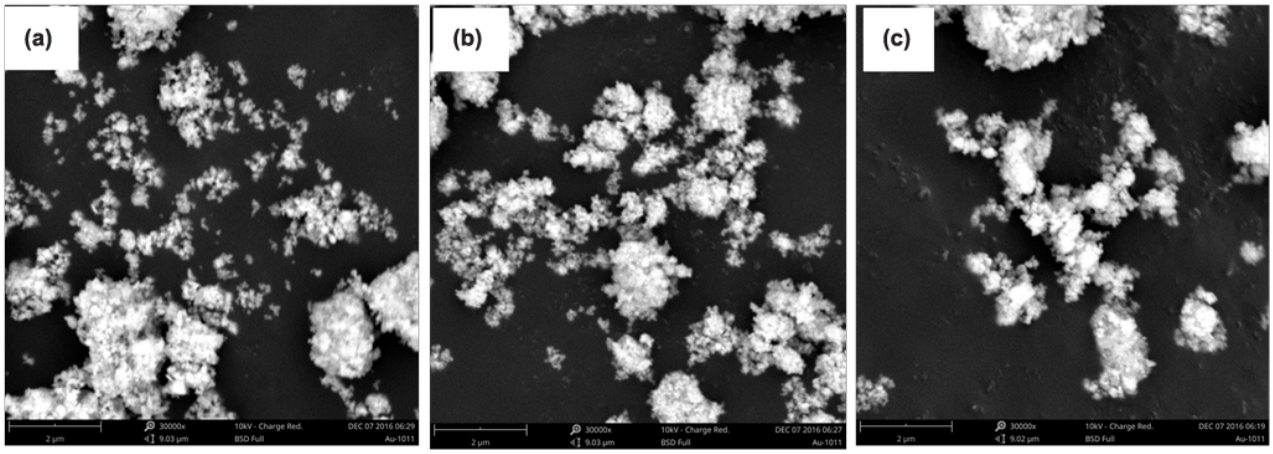


Fig. 3 — SEM images of $Bi_2WO_6$ samples [(a) BWO-MT; (b) BWO-DIW; (c) BWO-EG].

crystallite size and surface area. Smaller crystallite size means a shorter diffusion distance for the photogenerated electrons and holes, while large BET surface area can increase the contact area between the reactant and photocatalyst and provide more active sites during the photocatalytic process. Since BWO-EG sample has both advantages, it is reasonable to expect that it has a higher photocatalytic activity.

**Photocatalytic properties**

As an abundant class of synthetic, colored compounds, dyes present a danger to the environment because of their toxicity and stability. Hence these organic pollutants need to be mineralized over semiconductors which are used as photocatalysts. The adsorption abilities and the photodegradation activities of the various $Bi_2WO_6$ samples were evaluated by the adsorption and the photocatalytic degradation of MB dye, respectively.

As shown in Fig. 4, the adsorption abilities of the various $Bi_2WO_6$ samples were tested by the adsorption of MB under dark conditions. From the adsorption curves, it can be seen that the adsorption of MB become stable after 30 min, indicating that the adsorption-desorption equilibrium of the as-prepared $Bi_2WO_6$ samples is established in 30 min. Among the studied samples, BWO-EG exhibits the best adsorption ability, reaching 41.3% in 120 min, followed by BWO-DIW and BWO-MT, which is consistent with the BET results. So these results show that the higher adsorption is closely related to higher surface area, since higher surface area means more active sites that are beneficial for adsorption of MB.

Figure 5 displays the performance of MB photodegradation in the presence of different $Bi_2WO_6$ photocatalysts. In the absence of photocatalyst, the

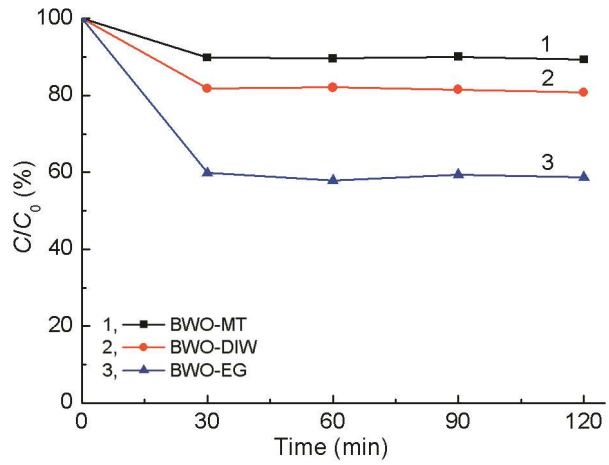


Fig. 4 — Adsorption of MB in the presence of different $Bi_2WO_6$ samples.

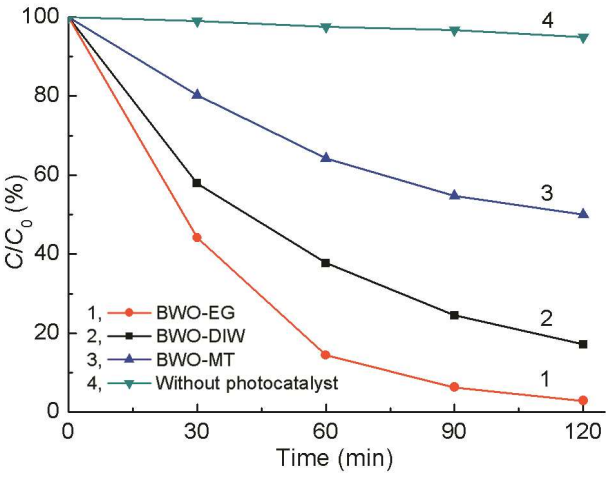


Fig. 5 — The performance of MB photodegradation in the presence of different $Bi_2WO_6$ samples.

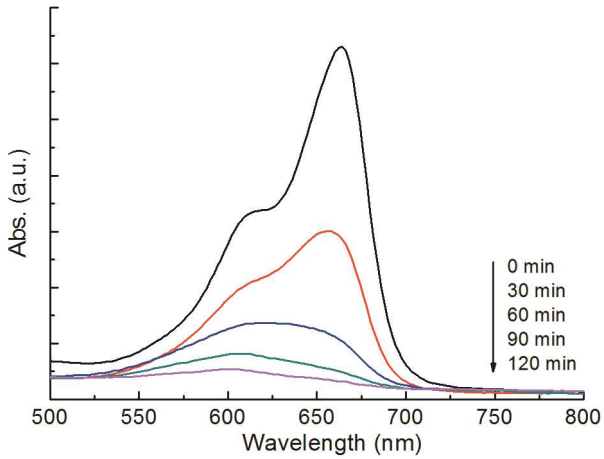


Fig. 6 — Evolution of UV-vis spectra over reaction time using BWO-EG as photocatalyst.

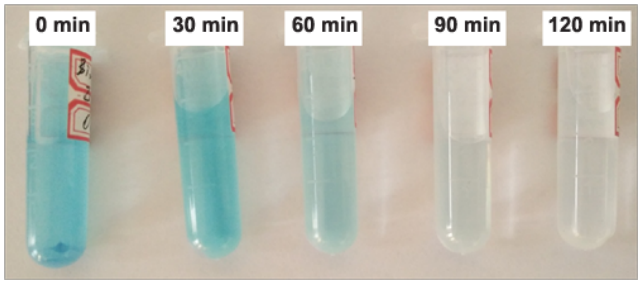


Fig. 7 — Color change of the MB solution over reaction time with BWO-EG catalyst.

degradation of MB was rather slow, while the concentrations of MB reduced faster in the presence of all the three samples, indicating that these samples showed photocatalytic activities. It was also observed that MB was degraded gradually with the increase of irradiation time for all the samples. After 120 min irradiation, the degradation percentage of MB was about 97.1%, 82.8%, and only 50.0% for BWO-EG, BWO-DIW and BWO-MT, respectively. The as-prepared BWO-EG exhibited a much more excellent visible light photocatalytic activity than BWO-DIW and BWO-MT. This suggested that the as-obtained BWO-EG could represent good candidate for further applications in environmental purification.

Figure 6 shows the evolution of UV-vis spectra over reaction time with the BWO-EG sample as photocatalyst. The spectra shows that as the exposure time increases, the absorption peaks at 664 nm diminish gradually with the peaks showing a blue-shift. The blue-shift can be attributed to the de-ethylation of MB.[22] After exposure for 120 min, the absorption peaks almost disappeared, indicating the complete photocatalytic degradation of the MB dye. Also, the color of the MB solution changes from initial blue to transparent as the exposure time increases (Fig. 7).

Generally, a complete photocatalytic reaction process comprises four steps: light absorption and generation of carriers, organic adsorption, redox reaction, and, products release. Increasing the quantity of carriers, reducing their recombination and improving their migration rate can greatly increase the efficiency of photodegradation. The adsorption of organic matter on photocatalyst particles is also an important factor influencing the photocatalytic activity. Our experiments showed that the introducing of ethylene glycol during the process of $Bi_2WO_6$ synthesis was favorable for its photocatalytic performance. The possible reason can be ascribed to the energy band structures, small crystalline size and high BET surface area of the BWO-EG sample. Firstly, the BWO-EG catalyst possesses enhanced light absorbance in the entire visible light region, which indicates more photogenerated carriers. Secondly, when ethylene glycol is used as solvent, $Bi^{3+}$ reacts with ethylene glycol to produce the complex, such as $Bi_x(EG)_y(OH)_z$,[23] rather than $Bi^{3+}$ directly reacting with $WO_4^{2-}$ to form $Bi_2WO_6$ precipitate. As the temperature increases during the solvothermal process, the complex gradually releases $Bi^{3+}$ and $WO_4^{2-}$, and then the $Bi_2WO_6$ crystallization reaction occurs. Therefore, due to the mild process of nucleation and growth, BWO-EG sample showed a much smaller crystallite size of ~9.2 nm as compared to of BWO-DIW (14.5 nm) and BWO-MT (26.5 nm). When the crystallite size is small, the migration distance of carriers from bulk to surface is short, and the recombination probability of carriers is greatly reduced. Thus more carriers can migrate to the reaction sites to degrade organic molecules rapidly.[24] Lastly, it is well-known that the surface area of photocatalyst is related to its photocatalytic activities.[25] When the surface area is large, more reaction sites are created and more dye molecules are adsorbed and then degraded on the surface of the photocatalyst, leading to a high photocatalytic performance. Therefore, when visible light energy stroked the $Bi_2WO_6$ sample, carriers were generated in the valence and conduction bands. The carriers migrate to the surface of $Bi_2WO_6$ and reacted with the adsorbed $O_2$ and $OH^-$ to produce $O_2^-$ and ·OH radicals. These $O_2^-$ and ·OH radicals then decomposed the MB molecules into $CO_2$ and $H_2O$.

## Conclusions

In summary, using ethylene glycol as the reaction medium, orthorhombic $Bi_2WO_6$ with the average crystallite size of ~9.2 nm and surface area of 56.5 $m^2\ g^{-1}$ was successfully synthesized by a simple solvothermal method. The as-prepared $Bi_2WO_6$ nanocrystals show excellent photodegradation activity of MB under visible light irradiation. This high photocatalytic activity is because of its energy band structures, small crystallite size and high BET surface area.

## Acknowledgement

The author gratefully acknowledges the financial support of the National Natural Science Foundation of China (No. 51471082, 61404071), the Key Program of Colleges and Universities in Henan Province (No. 15A430001) and the Foundation of Luoyang Normal University for Fostering National Program of China, PR China (No. 2014-PYJJ-002).

## References

1 Zhang K & Guo L J, *Catal Sci Technol*, 3 (2013) 1672.
2 Yang L L, Zhou H, Fan T X & Zhang D, *Phys Chem Chem Phys*, 16 (2014) 6810.
3 Yue D T, Qian X F & Zhao Y X, *Sci Bull*, 60 (2015) 1791.
4 Nakata K & Fujishima A, *J Photochem Photobiol C*, 13 (2012) 169.
5 Dozzi M V & Selli E, *J Photochem Photobiol C*, 14 (2013) 13.
6 Yao Z P, He Y Q, Xia Q X, Wei H & Jiang Z H, *RSC Adv*, 6 (2016) 51997.
7 Xue F, Fu W L, Liu M C, Wang X X, Wang B & Guo L J, *Int J Hydrogen Energy*, 41 (2016) 20455.
8 Peng S Q, Dan M, Guo F J, Wang H M & Li Y X, *Colloid Surf A*, 504 (2016) 18.
9 Kako T, Meng X G & Ye J H, *Appl Catal A*, 488 (2014) 183.
10 Hua X, Jin Y J, Wang K, Li N, Liu H Q, Chen M D, Paul S, Zhang Y, Zhao X D & Teng F, *Catal Commun*, 52 (2014) 45.
11 Sun S M, Wang W Z, Jiang D, Zhang L, Li X M, Zheng Y L & An Q, *Nano Res*, 7 (2014) 1497.
12 Li C M, Chen G, Sun J X, Rao J C, Han Z H, Hu Y D & Zhou Y S, *ACS Appl Mater Inter*, 7 (2015) 25716.
13 Saison T, Gras P, Chemin N, Chanéac C, Durupthy O, Brezová V, Colbeau-Justin C & Jolivet J P, *J Phys Chem C*, 117 (2013) 22656.
14 Huang H W, Liu K, Chen K, Zhang Y L, Zhang Y H & Wang S C, *J Phys Chem C*, 118 (2014) 14379.
15 Kudo A & Hijii S, *Chem Lett*, 28 (1999) 1103.
16 Zhang P, Hua X, Teng X X, Liu D S, Qin Z H & Ding S M, *Mater Lett*, 185 (2016) 275.
17 Zhao G, Liu S W, Lu Q F & Xiu Z L, *J Nanopart Res*, 15 (2013) 2121.
18 Liu S J, Hou Y F, Zheng S L, Zhang Y & Wang Y, *CrystEngComm*, 15 (2013) 4124.
19 Wang X J, Wan X L & Chang L L, *Catal Lett*, 144 (2014) 1268.
20 Madhusudan P, Yu J G, Wang W G, Cheng B & Liu G, *Dalton Trans*, 41 (2012) 14345.
21 Zhang X H, Zhao J G & Guo L J, *J Alloy Comp*, 582 (2014) 617.
22 Mu J J, Zheng G H & Ma Y Q, *J Electron Mater*, 46 (2017) 596.
23 Liu H Q, Gu X N, Chen F & Zhang J L, *Chin J Catal*, 32 (2011) 129.
24 Peng Y, Wang D, Zhou H Y & Xu A W, *CrystEngComm*, 17 (2015) 3845.
25 Song X C, Li W T, Huang W Z, Zhou H, Yin H Y & Zheng Y F, *J Nanopart Res*, 17 (2015) 134.